Isotope effect on the stereodynamics for the collision reaction H+LiF($v = 0$, $j = 0$)→ HF+Li *

Yue Xian-Fang(岳现房)†

Department of Physics and Information Engineering, Jining University, Qufu 273155, *China*

(Received 20 November 2011; revised manuscript received 4 February 2012)

Stereodynamics for the reaction H+LiF($v = 0$, $j = 0$) → HF+Li and its isotopic variants on the ground-state ($1^2A'$) potential energy surface (PES) are studied by employing the quasi-classical trajectory (QCT) method. At a collision energy of 1.0 eV, product rotational angular momentum distributions $P(\theta_r)$, $P(\phi_r)$, and $P(\theta_r, \phi_r)$, are calculated in the center-of-mass (CM) frame. The results demonstrate that the product rotational angular momentum $\boldsymbol{j}'$ is not only aligned along the direction perpendicular to the reagent relative velocity vector $\boldsymbol{k}$, but also oriented along the negative y axis. The four generalized polarization-dependent differential cross sections (PDDCSs) are also computed. The $PDDCS_{00}$ distribution shows a preferential forward scattering for the product angular distribution in each of the three isotopic reactions, which indicates that the title collision reaction is a direct reaction mechanism. The isotope effect on the stereodynamics is revealed and discussed in detail.

Keywords: stereodynamics, quasi-classical trajectory, isotope effect, polarization-dependent differential cross-section

PACS: 34.50.Lf, 82.20.Fd, 82.20.Hf **DOI:** 10.1088/1674-1056/21/7/073401

1. Introduction

Since the pioneering work of Herschbach *et al.*[1] and Zare *et al.*,[2] stereodynamics study of collision reactions have been predicted to provide valuable information in understanding the elementary reaction. Two factors make this proposed research develop quickly. One is the rapid development and application of the crossed molecule beam, polarized laser, and velocity ion imaging techniques, which allow the reliable and precise measurements of the product angular distribution and product angular momentum polarization effects. From the start of the research on measuring the product angular momentum polarization effects with polarized laser technique by Zare and coworkers,[3] there has been increasing interest in measuring angular momentum polarization effects in a variety of collision processes.[4,5]

The other factor which makes the research prosperous is the overall development of methods for computing product angular momentum polarization over the last one and a half decades. The methods involve the exploration of quantum mechanical (QM) formalism to study polarization in bimolecular reactions by Miranda and Clary,[6] and the quasi-classical trajectory (QCT) method developed by Han and coworkers.[7,8] With these methods, QM and QCT stereodynamical calculations on the reactions Cl+H_2,[9] O+HF,[10] and N+H_2[11] have been performed. All of these calculations pointed to rich dynamical behaviors that measurements of angular momentum polarization should potentially expose. The QCT studies, in particular, have highlighted the power of determining the product angular momentum polarization.[12]

The collision reaction Li+HF→LiF+H has become a benchmark for stereodynamics study from both experimental and theoretical points of view. This is because the reaction is one of the lightest reaction involving three different atoms, allowing quite reliable potential energy surface calculations for the ground[13] and excited states.[14] Crossed molecular beam[15] and transition state spectroscopic[16]studies have been performed from an experimental point of view. The electronic curve crossings and nonadiabatic couplings have also been investigated by simulating the spectroscopic processes. From a theoretical point of view, a number of QCT,[17,18] time-independent quantum dynamics,[19] and time-dependent wave packet calculations[20] have been carried out to explore the collision reaction processes. However, for its reverse collision reaction H+LiF→HF+Li, there is almost no study reported to the best knowledge of the au-

*Project supported by the National Natural Science Foundation of China (Grant No. 21003062).

†Corresponding author. E-mail: xfyuejnu@gmail.com

© 2012 Chinese Physical Society and IOP Publishing Ltd

thor, except for one quantum scattering calculation at collision energy ranging from 10^{-7} to 10^{-1} eV.[21] In the present work, stereodynamics studies are carried out for the collision reactions H+LiF→HF+Li, D+LiF→DF+Li, and T+LiF→TF+Li. The isotope effect on the stereodynamics is also revealed and discussed.

2. Theory

The most popular and accurate ground-state (1^2A') potential energy surface (PES) is used in the present study, which was developed by Aguado *et al.*[13] The full potential is written in terms of a many-body expansion as

$$V_{\rm ABC} = \sum_{\rm A} V_{\rm A}^{(1)} + \sum_{\rm AB} V_{\rm AB}^{(2)}(R_{\rm AB}) + V_{\rm ABC}^{(3)}(R_{\rm AB}, R_{\rm AC}, R_{\rm BC}), \quad (1)$$

where the summations run over all the terms of a given type, and $V_A^{(1)}$ is the energy of atom A in its appropriate electronic state. Usually, $\sum_A V_A^{(1)} = 0$ is true for all the atoms in their ground state. $R_{\rm AB}$, $R_{\rm AC}$, and $R_{\rm BC}$ are distances between atoms A and B, A and C, as well as B and C, respectively. $V_{\rm AB}^{(2)}$ and $V_{\rm ABC}^{(3)}$ are the two-body and three-body energies, respectively. The interested reader can find details about the PES in Ref. [22].

The present calculations were performed by applying a standard QCT-stereodynamics procedure which was initially developed by Han and coworkers[7−9,23−25] and has been successfully used to study a great deal of collision reactions.[26−37] The classical Hamilton's equations are integrated numerically in three dimensions. The accuracy of the numerical integration is verified by checking the conservation of the total energy and the total angular momentum for every trajectory. In the calculation, batches of 200000 trajectories are run for each reaction and the integration step size is chosen to be 0.1 femtosecond. The trajectories start at an initial distance of 15 Å between the H/D/T atom and the CM of LiF molecules. The impact parameter b is optimized through the repeated computations with 200000 trajectories for all of the present studies. The maximum impact parameter $b_{\rm max}$ is obtained when there is no reactive trajectory any more, if a bit larger value of b is increased. The optimized maximum impact parameters are 1.557, 1.560, and 1.565 Å for reactions H+LiF → HF+Li, D+LiF→DF+Li, and T+LiF→TF+Li, respectively. The collision energy is chosen to be 1.0 eV for all three reactions. The vibrational and rotational levels of the reagent molecule LiF are taken to be $v = 0$ and $j = 0$, respectively. The atom mass is chosen to be 6.941 u for Li, 18.9984 u for F, 1.008 u for H, 2.014 u for D, and 3.016 u for T, respectively.

The center-of-mass (CM) frame has been used as the reference frame in the present study, which is depicted in Fig. 1. The reagent relative velocity vector $\boldsymbol{k}$ is parallel to the z axis. The xz plane is the scattering plane which contains the initial and final relative velocity vectors, $\boldsymbol{k}$ and $\boldsymbol{k'}$. The $\theta_{\rm t}$ is the angle between the reagent relative velocity and the product relative velocity (so-called scattering angle). The $\theta_{\rm r}$ and $\phi_{\rm r}$ are the polar and azimuthal angles of the final rotational angular momentum $\boldsymbol{j'}$ The general theory of the product rotational polarization is standard.[8,9]

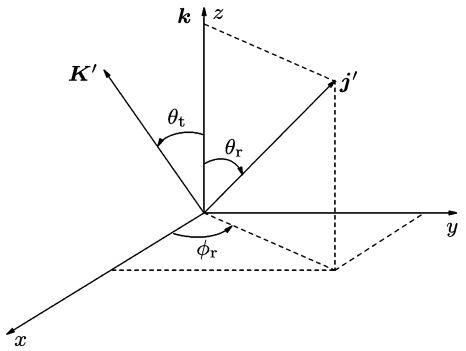


Fig. 1. Center-of-mass coordinate system used to describe $\boldsymbol{k}$, $\boldsymbol{k'}$, and $\boldsymbol{j'}$ correlations.

The distribution function $P(\theta_{\rm r})$ describing the $\boldsymbol{kj'}$ correlation can be expanded as a series of Legendre polynomials

$$P(\theta_{\rm r}) = \frac{1}{2}\sum_k [k] a_0^k P_k(\cos\theta_{\rm r}), \quad (2)$$

where $[k] = 2k + 1$. The coefficients a_0^k are given by

$$a_0^k = \langle P_k(\cos\theta_{\rm r})\rangle. \quad (3)$$

The expanding coefficients a_0^k are called orientation (k is odd) and alignment (k is even) parameters.

The dihedral angle distribution function $P(\phi_{\rm r})$ describing $\boldsymbol{k - k' - j'}$ correlation can be expanded as Fourier series

$$P(\phi_{\rm r}) = \frac{1}{2\pi}(1 + \sum_{n=2m} a_n \cos n\phi_{\rm r} + \sum_{n=2m-1} b_n \sin n\phi_{\rm r}), \quad (4)$$

where $m = 1, 2, \ldots$, $a_n = 2\langle\cos n\phi_{\rm r}\rangle$, and $b_n = 2\langle\sin n\phi_{\rm r}\rangle$.

The joint probability density function of angles θ_r and ϕ_r, which determine the direction of $\boldsymbol{j'}$, can be written as

$$\begin{aligned} P(\theta_r, \phi_r) &= \frac{1}{4\pi} \sum_{kq} [k] a_q^k C_{kq}(\theta_r, \phi_r)^* \\ &= \frac{1}{4\pi} \sum_{k} \sum_{q \geq 0} \left[a_{q\pm}^k \cos q\phi_r - \mathrm{i} a_{q\mp}^k \sin q\phi_r \right] \\ &\quad \times C_{kq}(\theta_r, 0), \end{aligned} \tag{5}$$

where

$$C_{kq} = \left(\frac{4\pi}{2k+1}\right)^{1/2} Y_{kq}(\theta, \phi)$$

are modified spherical harmonics. The full three-dimensional angular distribution associated with $\boldsymbol{k} - \boldsymbol{k'} - \boldsymbol{j'}$ correlation can be represented by a set of generalized polarization-dependent differential cross sections (PDDCSs) in the CM frame. The fully correlated CM angular distribution is written as

$$P(\omega_t, \omega_r) = \sum_{kq} \frac{[k]}{4\pi} \frac{1}{\sigma} \frac{\mathrm{d}\sigma_{kq}}{\mathrm{d}\omega_t} C_{kq}(\theta_r, \phi_r)^*, \tag{6}$$

where σ is the integral cross section, and $\sigma^{-1}\mathrm{d}\sigma_{kq}/\mathrm{d}\omega_t$ is a generalized PDDCS. In the present work, PDDCS$_{00}$ $(2\pi\sigma^{-1}\mathrm{d}\sigma_{00}/\mathrm{d}\omega_t)$, PDDCS$_{20}$ $(2\pi\sigma^{-1}\mathrm{d}\sigma_{20}/\mathrm{d}\omega_t)$, PDDCS$_{22+}$$(2\pi\sigma^{-1}\mathrm{d}\sigma_{22+}/\mathrm{d}\omega_t)$, and PDDCS$_{21-}$$(2\pi\sigma^{-1}\mathrm{d}\sigma_{21-}/\mathrm{d}\omega_t)$ are calculated. In the calculations, $P(\theta_r)$, $P(\phi_r)$, $P(\theta_r, \phi_r)$, and PDDCSs are expanded up to $k = 18$, $n = 24$, $k = 7$, and $k = 7$, respectively, showing a good convergence.

3. Results and discussion

Figure 2 displays the calculated product $P(\theta_r)$ distributions of the reactions H+LiF→HF+Li, D+LiF→DF+Li, and T+LiF→TF+Li, respectively. Clearly, each $P(\theta_r)$ distribution of these reactions is symmetric with respect to $\theta_r = 90°$, and shows a distinct peak at $\theta_r = 90°$. This indicates that the product rotational angular momentum vector $\boldsymbol{j'}$ is aligned perpendicular to the relative velocity direction $\boldsymbol{k}$. As shown in Fig. 2, the value of $P(\theta_r)$ at about $\theta_r = 90°$ becomes higher with the reaction changing from H+LiF→HF+Li to D+LiF→DF+Li. However, it becomes lower for the reaction T+LiF→TF+Li compared with the reaction D+LiF→DF+Li. This means that the change of the product alignment is not monotonic with increasing isotopic mass. As discussed by Wang *et al.*,[8,23] the $P(\theta_r)$ is sensitive to two factors: one is the character of the PES, and the other is the mass factor $\cos^2\beta$. The angle β is defined through the relation $\cos^2\beta = (m_A m_C)/[(m_A+m_B)(m_B+m_C)]$ for the reaction A+BC → AB+C). In the present study, the mass factor $\cos^2\beta$ is 0.013, 0.026, and 0.037 for the reactions H+ LiF→HF+Li, D+LiF→DF+Li, and T+LiF→TF+Li, respectively, which shows a monotonous change. Therefore, the product rotational alignment is affected not only by the mass factor, but also the PES.

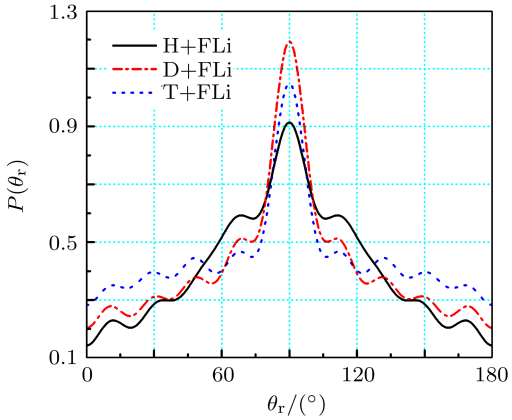


Fig. 2. (colour online) Distributions of $P(\theta_r)$ as a function of the polar angle θ_r for the reactions H+LiF→ HF+Li, D+LiF→DF+Li, and T+LiF→TF+Li.

Under the ϕ_r definition of the dihedral angle between the planes consisting of $\boldsymbol{k} - \boldsymbol{k'}$ and $\boldsymbol{k} - \boldsymbol{j'}$, the $P(\phi_r)$ distribution can provide both product rotational alignment and orientation information. Figure 3 displays the $P(\phi_r)$ distributions for the reactions H+Li→HF+Li, D+ LiF→DF+Li, and T+LiF→TF+Li.

A common feature is apparently disclosed in these three reactions that the distribution illustrate asymmetric properties about the scattering $\boldsymbol{k} - \boldsymbol{k'}$ plane, with one broad large peak appearing around $\phi_r = 270°$ and one small (or no) peak at about $\phi_r = 90°$, respectively. This feature conveys the information to us that most products tend to align along the direction of y axis which is perpendicular to the scattering $\boldsymbol{k} - \boldsymbol{k'}$ plane, and the orientation of the product rotational angular momentum tends to point to the direction of negative y axis. That is to say, the product molecules prefer a counterclockwise rotation (see from the direction of negative y axis) in the plane parallel to the scattering plane. As shown in Fig. 3, the $P(\phi_r)$ distribution at about $\phi_r = 270°$ shows a slightly decreasing trend with the increase of isotopic mass. At about $\phi_r = 90°$, the $P(\phi_r)$ distribution is almost the same for the reaction H+LiF→ HF+Li and D+LiF→DF+Li, but illustrates a tiny peak for

the reaction T+LiF→TF+Li. This indicates that the product rotational orientation becomes slightly weaker with the increase of isotopic mass.

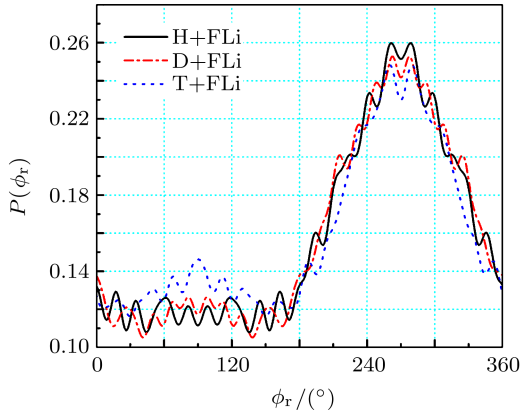


Fig. 3. (colour online) Distributions of $P(\phi_r)$ as a function of the dihedral angle ϕ_r for the reactions H+LiF→HF+Li, D+LiF→DF+Li, and T+LiF→TF+Li.

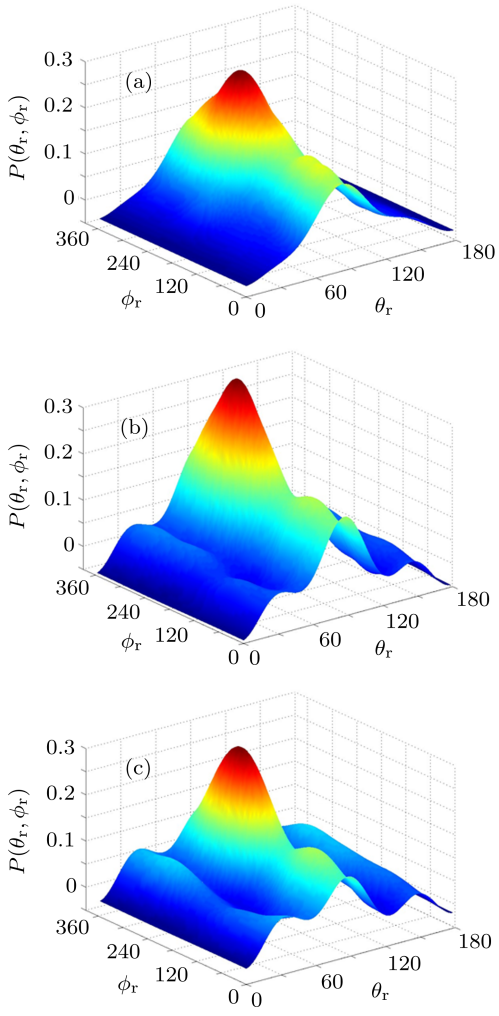


Fig. 4. (colour online) Distributions of $P(\theta_r, \phi_r)$ as a function of both the polar angle θ_r and dihedral angle ϕ_r for the reactions (a) H+LiF→HF+Li, (b) D+LiF→ DF+Li, and (c) T+LiF→TF+Li.

Alternative representation can provide complementary pictures of the scattering event which can lead to a further understanding of the mechanism governing molecular collision processes. The use of these alternative representations can help elucidate the stereodynamics information. As an alternative representation, the joint $P(\theta_r, \phi_r)$ distributions are displayed in Figs. 4(a), 4(b), and 4(c) for the reactions H+LiF→HF+Li, D+LiF→DF+Li, and T+LiF→TF+Li, respectively. The tomographical features are in good consistence with the separate $P(\theta_r)$ and $P(\phi_r)$ distributions.

The generalized PDDCSs describe the $\boldsymbol{k}-\boldsymbol{k'}-\boldsymbol{j'}$ correlation and the scattering direction of the product molecule. Figure 5 shows the calculated results of the PDDCSs for the reactions H+LiF→HF+Li, D+LiF→DF+Li, and T+LiF→TF+Li. The $\mathrm{PDDCS_{00}}$ is simply proportional to the differential cross section (DCS), and only describes the $\boldsymbol{k}-\boldsymbol{k'}$ correlation or the product angular distributions. Figure 5(a) presents the $\mathrm{PDDCS_{00}}$ as a function of the scattering angle θ_t for the above reactions. As clearly seen in Fig. 5(a), the $\mathrm{PDDCS_{00}}$ distributions are different for these three isotope reactions. For the reaction H+LiF→HF+Li, the $\mathrm{PDDCS_{00}}$ distribution shows a forward and sideways scattering, with a preference of forward scattering peaked at about $\theta_t = 35^\circ$. Comparatively, the $\mathrm{PDDCS_{00}}$ distribution mainly shows forward scattering for the reaction D+LiF→DF+Li, with the largest peak at about $\theta_t = 24^\circ$. It is remarkable that the $\mathrm{PDDCS_{00}}$ distribution shows both forward and backward scatterings for the reaction T+LiF→TF+Li, with a dominant forward scattering from $\theta_t = 0^\circ$ to 30°. These $\mathrm{PDDCS_{00}}$ distributions are characteristics of the direct reaction mechanism. To gain insight into the reaction mechanism, the variation of internuclear distances of H(D, T)-F, Li-F, and H(D, T)-Li with the propagation time are presented in Fig. 6. Trajectories are selected in scattering angle ranges of 30°–40°, 105°–115°, and 165°–175° for the reaction H+LiF→HF+Li; 20°–30°, 105°–115°, and 165°–175° for the reaction D+LiF→DF+Li; 0°–10°, 105°–115°, and 165°–175° for the reaction T+LiF→TF+Li, respectively. Most trajectories propagate with time in a similar way as that in Figs. 6(a), 6(b), and 6(c), which indicates that the H/D/T atoms collide with the LiF molecules and the HF/DF/TF products that move

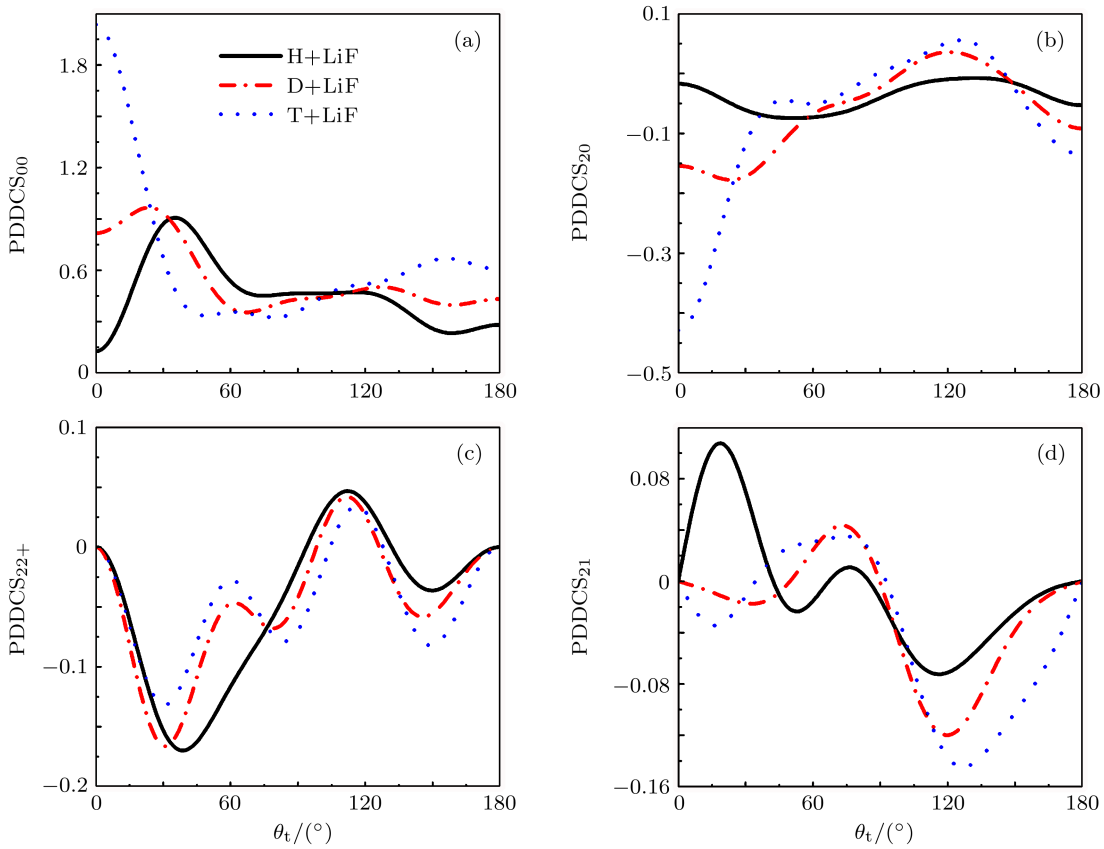


Fig. 5. (colour online) PDDCSs for (a) $(k,q)=(0,0)$, (b) $(k,q)=(2,0)$, (c) $(k,q\pm)=(2,2+)$, and (d) $(k,q^{\pm})=(2,1-)$.

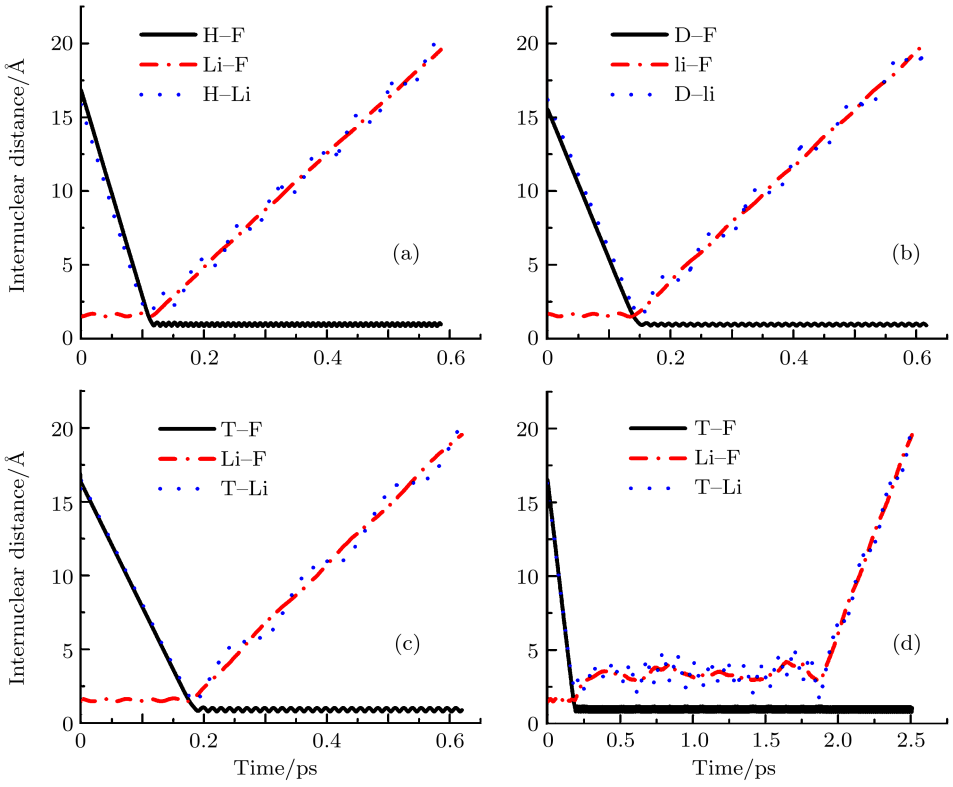


Fig. 6. (colour online) Internuclear distance of H(D, T)–F, Li–F, and H(D, T)–Li as a function of propagation time for the interaction (a) H+LiF→HF+Li at $\theta_t = 35°$, (b) D+LiF→DF+Li at $\theta_t = 24°$, (c) T+LiF→TF+Li at $\theta_t = 4°$, (d) T+LiF→TF+Li at $\theta_t = 7°$.

away immediately are formed. This discloses a direct dynamical process. Interestingly, a few indirect reactive trajectories are also observed in the calculated results. As an example, Fig. 6(d) depicts an indirect trajectory for the reaction T+LiF→TF+Li at the scattering angle $\theta_t = 7°$. As reported in Ref. [17], for the reaction H+LiF→HF+Li, the ground-state PES firstly shows a small barrier of 0.151 eV, and then a deep well of –0.361 eV in the minimum energy reaction path. The deep well allows any long-lived complex to form in the product channel, which can interpret the observed indirect trajectory displayed in Fig. 6(d). As shown in Fig. 6(d), lifetime of several picoseconds for the long-term complex may suffer few rotational periods before breaking into products, resulting in random scattering directions for the products. However, the calculated results show that the $PDDCS_{00}$ distribution are prominent forward scattering for all three reactions, which indicates that the title reaction mainly undergoes a direct reaction mechanism.

The $PDDCS_{20}$ distribution demonstrates an opposite trend to that of the $PDDCS_{00}$, which may result from the fact that the $PDDCS_{20}$ is related to alignment moment $\langle P_2(\cos\theta_r)\rangle$. When the product rotational angular momentum $\boldsymbol{j'}$ is perpendicular to $\boldsymbol{k}$, the $PDDCS_{20}$ is close to –0.5. For the reaction H+LiF→HF+Li, the $PDDCS_{20}$ values are negative for all scattering angles, but larger than –0.007, which suggests that the product rotational angular momentum $\boldsymbol{j'}$ polarizes preferentially along the direction perpendicular to $\boldsymbol{k}$. This is consistent with the product alignment prediction of the $P(\theta_r)$ distribution displayed in Fig. 2. However, for the reaction D+LiF→DF+Li, the $PDDCS_{20}$ values are negative for both backward and forward scatterings, but positive for the sideways scattering in the range of $\theta_t = 99° - 143°$. By comparison, the $PDDCS_{20}$ is a larger negative value for both backward and forward scatterings, but a larger positive value for the sideways scattering for the reaction T+LiF→TF+Li. This phenomenon may interpret that the alignments of the DF and TF products are stronger than that of the HF, but with the strongest alignment of the DF product, as shown in Fig. 2.

Figures 5(c) and 5(d) show the PDDCS distributions with $q \neq 0$. All of the PDDCSs with $q \neq 0$ are equal to zero at the ends of forward and backward scatterings. At these limits of scattering angle, the $\boldsymbol{k} - \boldsymbol{k'}$ scattering plane is not determined and the values of the PDDCSs with $q \neq 0$ must be zero. The behavior of PDDCSs with $q \neq 0$ at scattering angles $0^o < \theta_t < 180^o$ is more interesting, due to that they can provide detailed information about the product rotational alignment and orientation. The $PDDCS_{22+}$ is related to $\langle \sin^2\theta_r \cos 2\phi_r\rangle$. The negative values of the $PDDCS_{22+}$ correspond to the product rotational alignment along the y axis, while the positive values to the rotational alignment along the x axis. The larger the absolute value is, the stronger the product rotational alignment is along the corresponding axis. As shown in Fig. 5(c), the $PDDCS_{22+}$distribution for each reaction shows prominent large peaks at negative values around $\theta_t = 30°$, and the other prominent peaks around $\theta_t = 115°$ at positive values. This demonstrates that the product $\boldsymbol{j'}$ alignment is not only along the y axis, but also along the x axis, which is consistent with the $P(\theta_r)$ (see Fig. 2) and $P(\phi_r)$ (see Fig. 3) distributions. The $PDDCS_{21-}$ is related to $\langle -\sin 2\theta_r \cos\phi_r\rangle$, and its behavior is similar with that of the $PDDCS_{22+}$. The positive or negative $PDDCS_{21-}$ corresponds to the product rotational angular momentum $\boldsymbol{j'}$ along the direction of vector $\boldsymbol{x}-\boldsymbol{z}$ or $\boldsymbol{x}+\boldsymbol{z}$. As shown in Fig. 5(d), the $PDDCS_{21-}$ values vary with the scattering angle, which implies that the product angular momentum distribution is anisotropic. The $PDDCS_{21-}$ distributions show the largest negative peaks at $\theta_t = 117°$ for the reaction H+LiF→HF+Li, at $\theta_t = 120°$ for the reaction D+LiF→DF+Li, and at $\theta_t = 127°$ for the reaction T+LiF→TF+Li, respectively. This feature demonstrates that the rotational alignment of the HF/DF/TF products is along the $\boldsymbol{x}+\boldsymbol{z}$ direction. The peak shows an increasing trend with the increase of isotopic mass. Another notable character in Fig. 5(d) is that the largest positive peak is at $\theta_t = 20°$ for the reaction H+LiF→HF+Li, which is not found in the other two reactions. This illuminates that the rotational alignment of the HF product is also mainly along the $\boldsymbol{x} + \boldsymbol{z}$ direction. These results are likely to offer the reason why the $P(\theta_r)$ distribution of the HF product is weaker than that of the DF and TF products shown in Fig. 3.

4. Conclusion

Quasi-classical trajectory calculations are performed to investigate the stereodynamics for the reactions H+LiF→HF+Li, D+LiF→DF+Li, and T+LiF→TF+Li. Three commonly used angular momentum distributions $P(\theta_r)$, $P(\phi_r)$, and $P(\theta_r, \phi_r)$, as

well as four PDDCSs are explored. The $P(\theta_r)$ distribution shows a prominent peak at $\theta_r = 90°$, while the $P(\phi_r)$ distribution displays a broad large peak around $\phi_r = 270°$ and a very small peak around $\phi_r = 90°$ for all these three reactions, which indicates that the product rotational angular momentum $\boldsymbol{j'}$ is not only aligned along the direction perpendicular to the reagent relative velocity $\boldsymbol{k}$, but also oriented along the negative direction of the y axis. As an alternative representation, the joint distribution of $P(\theta_r, \phi_r)$ is consistent with the $P(\theta_r)$ and $P(\phi_r)$ distributions. Differential cross sections are revealed from the $PDDCS_{00}$ distributions, and illustrate preferential forward scatterings for all the HF, DF, and TF products, which is the characteristic of the direct reaction mechanism. Further calculations about the variations of internuclear distances along the propagation time also support the dominant direct reaction mechanism for the title reaction. The $PDDCS_{20}$ and $PDDCS_{22+}$ distributions are consistent with angular momentum distributions. The $PDDCS_{21-}$ distribution demonstrates that the product angular distributions are anisotropic.

References

[1] Mcclelland G M and Herschbach D R 1979 *J. Phys. Chem.* A **83** 1445

[2] Jonah C D, Zare R N and Ottinger C 1972 *J. Chem. Phys.* **56** 263

[3] Greene C H and Zare R N 1983 *J. Chem. Phys.* **78** 6741

[4] Han K L, He G Z and Lou N Q 1993 *Chem. Phys. Lett.* **203** 509

[5] Yan S, Wu Y T, Zhang B, Yue X F and Liu K 2007 *Science* **316** 1723

[6] de Miranda M P and Clary D C 1997 *J. Chem. Phys.* **106** 4509

[7] Han K L, He G Z and Lou N Q 1996*J. Chem. Phys.* **105** 8699

[8] Wang M L, Han K L and He G Z 1998 *J. Chem. Phys.* **109** 5446

[9] Chen M D, Han K L and Lou N Q 2003 *J. Chem. Phys.* **118** 4463

[10] Zhao J, Xu Y and Meng Q T 2009 *J. Phys.* B **42** 165006

[11] Yue X F, Cheng J, Li H, Zhang Y Q and Wu E L 2010 *Chin. Phys.* B **19** 043401

[12] de Miranda M P and Aoiz F J 2004 *Phys. Rev. Lett.* **93** 083201

[13] Aguado A, Paniagua M, Lara M and Roncero O 1997 *J. Chem. Phys.* **107** 10085

[14] Jasper A W, Hack M D, Truhlar D G and Piecuch P 2002 *J. Chem. Phys.* **116** 8353

[15] Becker C H, Casavecchia P, Teidemann P W, Valentini J J and Lee Y T 1980 *J. Chem. Phys.* **73** 2833

[16] Hudson A J, Oh H B, Polanyi J C and Piecuch P 2000 *J. Chem. Phys.* **113** 9897

[17] Cheng J and Yue X F 2011 *Chin. Phys. Lett.* **28** 083102

[18] Wang T and Yue X F 2011 *Chin. Phys. Lett.* **28** 023101

[19] Zhang J Z H and Miller W H 1989 *J. Chem. Phys.* **91** 1528

[20] Chen R and Guo H 1996 *J. Chem. Phys.* **105** 3569

[21] Weck P F and Balakrishnan N 2005 *J. Chem. Phys.* **122** 234310

[22] Aguado A, Paniagua M, Lara M and Roncero O 1997 *J. Chem. Phys.* **106** 1013

[23] Wang M L, Han K L and He G Z 1998 *J. Phys. Chem.* A **102** 20204

[24] Chen M D, Han K L and Lou N Q 2002 *Chem. Phys. Lett.* **357** 483

[25] Zhang X and Han K L 2006 *Int. J. Quant. Chem.* **106** 1815

[26] Liu S L and Shi Y 2011 *Chin. Phys.* B **20** 013404

[27] Liu Y F, Zhang W, Shi D H and Sun J F 2009 *Chin. Phys.* B **18** 4264

[28] Xu W W, Liu X G, Luan S X, Sun S S and Zhang Q G 2009 *Chin. Phys.* B **18** 339

[29] Chu T S, Zhang H, Yuan S P, Fu A P, Si H Z, Tian F H and Duan Y B 2009 *J. Phys. Chem.* A **113** 3470

[30] Liu Y F, He X H, Shi D H and Sun J F 2011 *Chin. Phys.* B **20** 078201

[31] Xu Y, Zhao J, Yue D G, Liu H, Zheng X Y and Meng Q T 2009 *Chin. Phys.* B **18** 5308

[32] Zhang W Q, Cong S L, Zhang C H, Xu X S and Chen M D 2009 *J. Phys. Chem.* A **113** 4192

[33] Ge M H and Zheng Y J 2011 *Chin. Phys.* B **20** 083401

[34] Li X H, Wang M S, Pino H, Yang C L and Ma L Z 2009 *Phys. Chem. Chem. Phys.* **11** 10438

[35] Zhao J, Xu Y and Meng Q T 2010 *Chin. Phys.* B **19** 063401

[36] Yue D G, Zheng X Y, Liu H and Meng Q T 2009 *Chin. Phys.* B **18** 1479

[37] Zhang W, Liu Y F and He X 2010 *Chem. Phys. Lett.* **489** 237